Optical pumping schemes for nuclear spin polarization of ^{35}Ar

F. Lenaers,[1] R. D. Glover,[2] and T. Bastin[1]

[1]*Institut de Physique Nucléaire, Atomique et de Spectroscopie, CESAM, Université de Liège, Bât. B15, B - 4000 Liège, Belgium*

[2]*Institute for Photonics and Advanced Sensing and School of Physical Sciences, The University of Adelaide, Adelaide, South Australia 5005, Australia*

(Received 17 August 2020; revised 9 December 2020; accepted 16 December 2020; published 11 January 2021)

Quantum-state preparation has a wide range of applications ranging from quantum optics to quantum metrology to fundamental physics precision measurements. In the context of nuclear β-decay correlation experiments such as the ones using argon, one needs to prepare a source of highly polarized atoms. Creating such a state-prepared sample amounts to generating a so-called stretched state, i.e., a state with the maximal projection of the total angular momentum along the quantization axis. This is typically achieved through optical pumping. Since this technique inherently depends on cycles of absorption followed by spontaneous emission, it may lead to undesirable heating and population loss. It is therefore crucial to devise polarization methods with both optimized efficiency and minimized drawbacks. We propose and compare various schemes, which we have been investigating numerically in the case of argon-35 atoms. We show that polarization degrees as high as 99.99% can be obtained within less than 140 μs.

DOI: 10.1103/PhysRevA.103.013105

I. INTRODUCTION

The standard model (SM) involves about 30 free parameters that need to be determined experimentally [1]. This means that the SM can be overconstrained and in principle tested to any desired accuracy. Indeed, the more precise the measurements of these parameters, the more precise the theoretical SM predictions, which, in turn, makes it possible to design experiments that are increasingly sensitive to deviations from SM predictions and thus to new physics beyond SM [2]. In terms of methods, laser cooling and trapping techniques provide well-controlled environments, which explains why several experiments have been and are being developed that use a magneto-optical trap (MOT) to prepare their source for precision tests [3–12].

Historically, the study of nuclear β decay has played a crucial role in the development of the electroweak standard model, and it continues to be a central field for precision tests of the SM [12–15]. The unitarity tests of the Cabibbo-Kobayashi-Maskawa (CKM) quark-mixing matrix are very sensitive probes to test the electroweak standard model and to search for signatures of new physics [15–17]. To date, the best precision is obtained from the top-row normalization test, i.e.,

$$|V_{ud}|^2 + |V_{us}|^2 + |V_{ub}|^2 = 1, \tag{1}$$

where the elements V_{ud}, V_{us}, and V_{ub} describe the mixing between the up quark (u) and the down-type quarks (d, s, and b). Since V_{ud} depends on the lightest quarks, it is the element that can be determined most precisely [18].

Traditionally, three sources have been used to deduce V_{ud}, namely, superallowed $0^+ \to 0^+$ pure Fermi transitions [19,20], neutron decay [2,21], and pion β decay [22]. Naviliat-Cuncic and Severijns [23] have shown that superallowed β transitions within isospin $T = 1/2$ doublets (often termed mirror transitions) could be used as an independent sensitive source to determine V_{ud}. Among these transitions, the mirror β decay of ^{35}Ar has been identified as a promising candidate [1]. The extraction of V_{ud} from mirror nuclei can make use of a spin-polarized sample [24], and in this context state preparation of ^{35}Ar atoms is a crucial issue. In this paper, we investigate this question in order to identify optimal polarization schemes for future use in precision measurements. Spin polarization can be achieved through different methods such as optical pumping [6–9,25–28], low-temperature orientation [29], projectile fragmentation [30], and beam interaction with a tilted foil [31]. When applicable, optical pumping can yield a high degree of spin polarization and it is particularly well adapted to implementation in a cold-atom setup, which is the focus of the work here. However, optical pumping can be applied more broadly: for example, at the versatile ion-polarized technique on-line (VITO) beam line at ISOLDE [28,32], a similar optical pumping scheme was investigated for spin polarizing an ^{35}Ar atomic beam. Instead of being trapped then polarized, atoms in this setup are polarized then implanted into a crystal host. We hope that discussing the matter from a cold-atom point of view will provide additional insights.

The paper is organized as follows. Section II reviews how V_{ud} is extracted from mirror transitions. Section III describes the model we used for studying the atom-field interaction and comparing the different polarization schemes in ^{35}Ar. Section IV presents the results of our numerical simulations and discusses the advantages of each method.

II. V_{ud} AND MIRROR TRANSITIONS

As is the case with superallowed $0^+ \to 0^+$ pure Fermi decay, extracting V_{ud} from a $T = 1/2$ mirror β transition

requires precise knowledge of the corresponding ft value [33]. In practice, a corrected $\mathcal{F}t$ value is introduced in order to take into account corrections due to undetected radiative effects (such as the emission of a Bremsstrahlung photon) as well as to isospin-symmetry breaking [19]. For mirror transitions, the relation between V_{ud} and $\mathcal{F}t$ is given by [23]

$$\mathcal{F}t^{\text{mirror}}\left(1+\frac{f_A}{f_V}\rho^2\right)=\frac{K}{G_{\text{F}}^2V_{ud}^2(1+\Delta_{\text{R}}^V)}. \tag{2}$$

Here, $K/(\hbar c)^6=2\pi^3\hbar\ln 2/(m_ec^2)^5$ and amounts to [34]

$$8120.276237(12)\times 10^{-10}\ \text{GeV}^{-4}\ \text{s}.$$

The constant G_{F} is the Fermi constant derived from the muon lifetime formula [2], Δ_R^V is the transition-independent part of the radiative correction, and f_A and f_V are the statistical rate functions for the axial-vector (A) and vector (V) parts of the interaction.

As is made clear by Eq. (2), extracting V_{ud} from a mirror β transition requires not only the determination of the $\mathcal{F}t$ value but also that of the mixing ratio ρ. The value of ρ needs to be deduced from the measurement of an observable that is a function of ρ. As is the case with neutron decay [35], three correlation coefficients can be considered, each providing transition-dependent sensitivities [1], namely, the β-ν angular correlation a, the β-asymmetry parameter A_β, and the ν-asymmetry parameter B.

All in all, two sources of uncertainties determine the precision that can be obtained for V_{ud} from mirror transitions: the uncertainty in the $\mathcal{F}t$ value and the uncertainty in the mixing ratio, which is itself determined by the precision reached when measuring the correlation coefficient. The value of V_{ud} extracted from the available data in the mirror decays of ^{19}Ne, ^{21}Na, ^{29}P, ^{35}Ar, and ^{37}K is [36]

$$|V_{ud}|=0.9743(14), \tag{3}$$

where the uncertainty, which is about eight times larger than in the case of superallowed pure Fermi transitions, is dominated by the uncertainties in the mixing ratios.

Severijns and Naviliat-Cuncic [1] have pointed out that measurement of A_β in the mirror β decay of ^{35}Ar would be the most sensitive of all correlation parameter measurements for mirror nuclei. Determining A_β for ^{35}Ar with a relative precision of 0.5% while improving the $\mathcal{F}t$-value precision by a factor of 4.8 would yield an absolute precision on V_{ud} of 0.0004, i.e., only about twice as much as the uncertainty of 0.00021 obtained from the set of superallowed pure Fermi transitions [1,2].

The β-particle angular distribution from the decay of a nuclear spin-polarized ensemble is given in leading order by [24]

$$W(\theta)\sim 1+A_\beta\frac{\langle\mathbf{I}\rangle}{I}\cdot\frac{\mathbf{p}_\beta c}{E_\beta}=1+A_\beta\frac{\langle I_z\rangle}{I}\frac{v}{c}\cos\theta, \tag{4}$$

where $\mathbf{p}_\beta$, E_β, and v are the momentum, the energy, and the velocity of the emitted β particle, $\langle\mathbf{I}\rangle/I$ is the expectation value of the nuclear spin polarization vector of the parent nucleus, and θ is the angle between the polarization z axis and the recoils [37].

From Eq. (4), it is clear that a measurement of A_β to a given relative precision requires the nuclear polarization to be known with at least equal precision. In the case of a high polarization degree such as $\langle I_z\rangle/I=99\%$, measuring $1-\langle I_z\rangle/I=10^{-2}$ with a relative precision of 20% would be enough to reach a relative precision of $\Delta(\langle I_z\rangle/I)/(\langle I_z\rangle/I)=0.2\%$.

To sum up, the procedure to extract V_{ud} from a given mirror β transition is: (i) The measurement of the β-asymmetry parameter A_β makes it possible to access the mixing ratio ρ. (ii) Together with the calculations of the statistical function f_V, the ratio f_A/f_V, and the various theoretical corrections introduced so far, the determination of ρ is used to determine the $\mathcal{F}t$ value. (iii) The value of V_{ud} is then extracted from Eq. (2).

Such a procedure has been successfully implemented by Fenker *et al.* [8,9] using the TRIUMF Neutral Atom Trap (TRINAT). They performed a 0.3% measurement of the β-asymmetry parameter A_β in the mirror β decay of ^{37}K,

$$A_\beta=-0.5707(13)_{\text{syst}}(13)_{\text{stat}}(5)_{\text{pol}}, \tag{5}$$

which is the nuclear A_β measurement with best relative accuracy [9]. Their result relies on crucial developments, which enabled them to determine the average nuclear polarization of their sample with a precision smaller than 0.1%, thus ensuring that the final uncertainty of A_β is not dominated by the polarization uncertainty. Fenker *et al.* [8] are confident that the polarization uncertainty could be further reduced down to ~0.04%. The TRINAT ^{37}K experiment highlights the potential of both MOT setups and optical pumping for precision measurements. As such it provides a benchmark for our own work with ^{35}Ar.

III. ^{35}Ar CASE

A. Level scheme

The mirror β decay of ^{35}Ar,

$$^{35}_{18}\text{Ar}\rightarrow{}^{35}_{17}\text{Cl}+e^+ +\nu_e, \tag{6}$$

occurs with a branching ratio of 98.16(5)% [38] to the stable ground state of the daughter nucleus $^{35}_{17}$Cl. This process has a half-life of $T_{1/2}=1.7756(10)$s [38], which is compatible with both the preparation of the sample and the collection of data. Argon has a ground-state electronic configuration $1s^22s^22p^63s^23p^6\equiv[\text{Ne}]3s^23p^6$. As is the case with other noble gases [39], the cooling and trapping of argon atoms is achieved by selecting an optically accessible closed transition whose effective ground state is a metastable excited state. Two of the first four excited states in the $[\text{Ne}]3s^23p^54s$ configuration, namely the $[1/2]_0$ and $[3/2]_2$ fine-structure states [38], are metastable, the former with a calculated lifetime of 44.9 s [40] and the latter with a measured lifetime of 38^{+8}_{-5} s [41]. The next set of excited states are in the $[\text{Ne}]3s^23p^54p$ configuration, and are all short lived. Out of the allowed transitions between these two sets, the $4s[3/2]_2\rightarrow 4p[5/2]_3$ transition at an air wavelength of $\lambda=811.5$ nm [42] is a closed one and hence of interest. Both stable ^{40}Ar and long-lived radioactive ^{39}Ar have been cooled and trapped using this transition [41,43–45]. In the following, the ground state (denoted g)

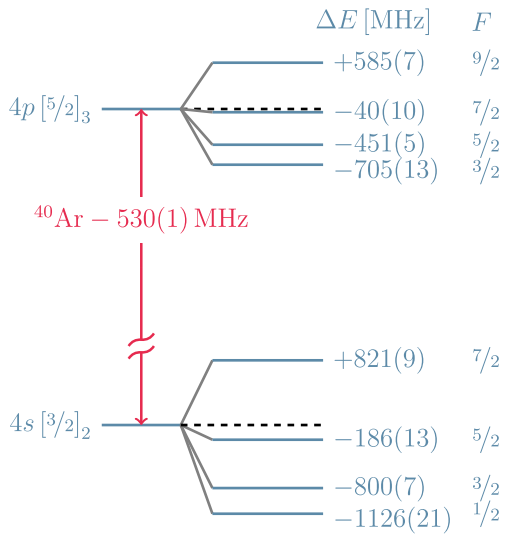

FIG. 1. Hyperfine structure of the 811.5 nm $4s[3/2]_2 \rightarrow 4p[5/2]_3$ transition of ^{35}Ar. The hyperfine splittings were calculated using the estimated values of the dipolar and quadrupolar hyperfine structure constants of Ref. [46]. The isotopic shift between ^{35}Ar and ^{40}Ar is an estimate from Ref. [46].

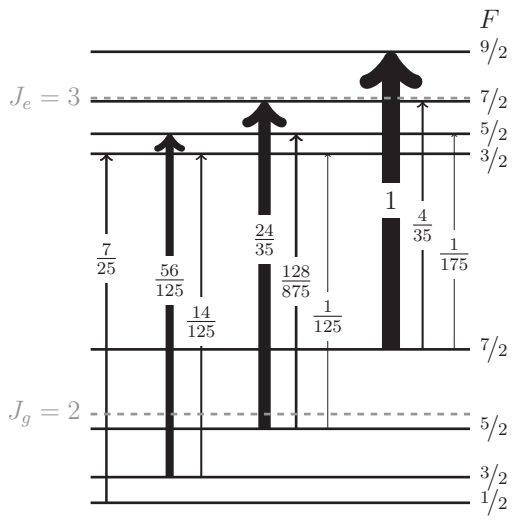

FIG. 2. Line strengths for the hyperfine-structure transitions involved in the $4s[3/2]_2 \rightarrow 4p[5/2]_3$ transition of ^{35}Ar, with respect to the most intense transition, $F_g = 7/2 \rightarrow F_e = 9/2$.

refers to the $4s[3/2]_2$ state, and the excited state (denoted e) refers to the $4p[5/2]_3$ state.

Argon-35 has a nuclear spin $I = 3/2$ whose interaction with the atomic electrons causes hyperfine splittings within each fine-structure state. Both the $4s[3/2]_2$ and $4p[5/2]_3$ states split into four hyperfine-structure components–with F going from 1/2 to 7/2 and from 3/2 to 9/2, respectively, as illustrated in Fig. 1.

It must be noted that the lifetimes mentioned above for the metastable states are those of the zero nuclear spin isotope ^{40}Ar. In the presence of a nonzero nuclear spin, as is the case with ^{35}Ar, one must pay attention to hyperfine-induced transitions (HIT), also referred to as hyperfine quenching decay modes, which are known to alter the lifetimes of metastable states [47–49]. The hyperfine interaction mixes a small amount of the short-lived $4s[1/2]_1$ and $4s[3/2]_1$ states into the metastable $4s[1/2]_0$ and $4s[3/2]_2$ states, thus opening additional decay channels to the ground state. In xenon, hyperfine quenching lifetime reduction from ∼43 s to ∼5 s have been measured [49]. In neon, similar orders of magnitude have been predicted [48]. Similar theoretical investigations of argon would be a welcome addition to the literature. That being said, one needs to keep in mind that the limiting timescale in a magneto-optical trap using ^{35}Ar will be the half-life of this isotope, i.e., $T_{1/2} \sim 2$ s [38].

In the presence of a magnetic field, each of the F hyperfine levels is further split up into $2F + 1$ magnetic sublevels ($m_F = -F, \ldots, F$). All in all, the hyperfine structure of the $4s[3/2]_2 \rightarrow 4p[5/2]_3$ transition comprises $N = 48$ magnetic sublevels. They are denoted hereafter by $|g$ or $e, F, m_F\rangle$, and the transition frequency between any two of these levels by $\nu_{\text{lower state}}^{\text{upper state}}$.

B. Polarization schemes

1. *Optical polarization schemes*

The atomic sample is fully polarized at the nuclear level if it is pumped into any electronic Zeeman sublevel $|F_{\max} = J + I, m_F = \pm F_{\max}\rangle$ [25]. We consider the case of trapped atoms in the $F_g = 7/2$ manifold, and we choose the maximally polarized ground-state $|7/2, {}^{+}7/2\rangle$ sublevel as our target state (we could have also chosen the $|7/2, {}^{-}7/2\rangle$ state). To this aim, more than one optical pumping scheme can be explored. We can either use one σ^+-pump laser on the $F_g = 7/2 \rightarrow F_e = 9/2$ transition (one-laser scheme), or use one σ^+-pump laser on the $F_g = 7/2 \rightarrow F_e = 7/2$ and one σ^+-repump laser on the $F_g = 5/2 \rightarrow F_e = 7/2$ transition (two-laser scheme).

An external homogeneous static magnetic field parallel to the z axis of propagation of the pumping light is also considered. The addition of such a field may inhibit uncontrolled Larmor precession [50]. In our case, the presence of a magnetic field is also helpful when highlighting and mitigating the effect of coherent population trapping (CPT) [8,51,52].

(a) One-laser scheme. In this configuration, the target state $|7/2, 7/2\rangle$ is a bright state. In other words, the laser keeps interacting with the atoms even after they have reached the target state. Such additional, unnecessary scattering processes might lead to undesirable heating and disruption of the trapping conditions.

(b) Two-laser scheme. In the two-laser configuration, the target state $|7/2, 7/2\rangle$ is a dark state, as is the case, for example, in the ^{37}K experiment [9]. To understand why this configuration has to involve two lasers, it is worth having a look at the characteristics of the $J_g = 2 \rightarrow J_e = 3$ transition (see Fig. 2). When an atom is excited to the $F_e = 9/2$ manifold, it has no choice but to decay to the $F_g = 7/2$. By contrast, if an atom is excited to the $F_e = 7/2$ manifold, it can decay either in the $F_g = 7/2$ manifold or in the $F_g = 5/2$ manifold, with the latter option being six times more likely. If the $F_g = 7/2 \rightarrow F_e = 7/2$ transition was not excited by a so-called repump laser,

the $F_g = 7/2$ manifold would end up being significantly depleted. Moreover, as compared with other transitions, the line strength of the $F_g = 7/2 \rightarrow F_e = 7/2$ transition is relatively weak.

When using a two-laser configuration, one should be mindful of coherent population trapping (CPT). This phenomenon can indeed affect the efficiency of optical pumping and lead to false polarization signal [8,51,52]. CPT arises in Λ-type systems, when two coherent laser beams excite transitions from two stable lower levels $|g_1\rangle$ and $|g_2\rangle$ to a common excited state $|e\rangle$ [27]. When the frequency difference between the two laser beams is equal to the frequency splitting between the two lower states, atoms are trapped in a dark, i.e., nonabsorbing-superposition state. In our two-laser scheme, the system of interest, i.e., the set of transitions addressed by the laser beams, is not a single three-level Λ system, but consists in a series of five Λ-type subsystems, which are interlinked through decay pathways. Whenever the frequency difference between the two lasers is equal to the frequency splitting between two ground-state Zeeman sublevels $|5/2,\, m_F\rangle$ and $|7/2,\, m_F\rangle$, some atoms are expected to be trapped in states other than the target state, thus hindering the process of optical pumping. We can identify six such frequency splittings, each of which gives rise to a CPT resonance. The values of these frequency splittings depend on Zeeman shifts, hence on the amplitude of the magnetic field. If the frequencies ν_1^{L} and ν_2^{L} of the two lasers are chosen so that they are in resonance with respect to the hyperfine splittings, i.e., $\nu_1^{\mathrm{L}} = \nu_{g,7/2}^{e,7/2}$, and $\nu_2^{\mathrm{L}} = \nu_{g,5/2}^{e,7/2}$, then their frequency difference

$$\delta\nu_{12}^{\mathrm{L}} \equiv \nu_2^{\mathrm{L}} - \nu_1^{\mathrm{L}} \tag{7}$$

is equal to the hyperfine splitting between the lower hyperfine manifolds $F_g = 5/2$ and $F_g = 7/2$:

$$\delta\nu_{12}^{\mathrm{L}} = \nu_{g,5/2}^{g,7/2} = 1007\ \mathrm{MHz}.$$

This matches the CPT condition when the amplitude of the magnetic field B is equal to zero—in that case, there is only one resonance since there is no Zeeman shift. Furthermore, for small nonzero values of B, $\delta\nu_{12}^{\mathrm{L}}$ is likely to be close to one of the CPT resonances.

2. Nuclear polarization degree

We characterize the nuclear spin polarization by the quantity

$$P_I = \frac{1}{I}\sum_{F=1/2}^{7/2}\sum_{m_F=-F}^{+F}\langle I_z\rangle_{|F,\,m_F\rangle}\rho_{(g,F,\,m_F),(g,F,\,m_F)}, \tag{8}$$

where $\langle I_z\rangle_{|F\,m_F\rangle} \equiv \langle F\, m_F|I_z|F\, m_F\rangle$ is the average nuclear spin projection associated with a given $|F\, m_F\rangle$ Zeeman sublevel. The operator I_z is diagonal in the uncoupled basis $\{|J\, m_J\rangle \otimes |I\, m_I\rangle\}$ with J (I) the electronic (nuclear) total angular momentum quantum number and m_J (m_I) the associated magnetic quantum number [25]. It is therefore convenient to rewrite the total-angular-momentum states $|F\, m_F\rangle$ as linear combinations of the $|J\, m_J\rangle \otimes |I\, m_I\rangle$ states using the transformation

$$|F\, m_F\rangle = \sum_{m_I,\,m_J}\langle J\, m_J\, I\, m_I|F\, m_F\rangle|J\, m_J\rangle \otimes |I\, m_I\rangle, \tag{9}$$

where $\langle J\, m_J\, I\, m_I|F\, m_F\rangle$ denote the Clebsch-Gordan coefficients. For the four ground-state manifolds, this yields

$$\langle I_z\rangle_{|F,\,m_F\rangle} = a_F\, m_F, \tag{10}$$

with $a_{7/2} = 3/7$, $a_{5/2} = 13/35$, $a_{3/2} = 1/5$, and $a_{1/2} = 1$. P_I is normalized so that its values range between -1 and $+1$; if the atoms are all in the stretched state $|7/2,\, {}^{+}7/2\rangle$ ($|7/2,\, {}^{-}7/2\rangle$), then P_I is equal to $+1$ (-1), while P_I is equal to zero when the atomic ensemble is equidistributed in the sublevels of the manifold.

In an experimental setup, P_I is not extracted from one optical pumping sequence. For example, in the TRINAT ^{37}K experiment [9], each duty cycle consists of a series of 100 subcycles, each of which consists in first polarizing the atoms then recollecting them with the magneto-optical trap. This duty cycle is itself repeated with the polarization of the optical pumping light being flipped. The system that we are modeling assumes that the trapped atoms are in the ground-state $F_g = 7/2$ manifold. It is therefore crucial to make sure that the amount of atoms, which are no longer in this manifold at the end of the optical pumping sequence, is kept as low as possible. To monitor this issue, we define the residual population, i.e., the population that is not in the ground-state $F_g = 7/2$ manifold, for both the one- (1L), and the two-laser (2L) schemes,

$$\rho_{\mathrm{res}}^{\mathrm{1L}} = 1 - \sum_{m_F=-9/2}^{9/2}\rho_{(e,\frac{9}{2},m_F),(e,\frac{9}{2},m_F)} - \sum_{m_F=-7/2}^{7/2}\rho_{(g,\frac{7}{2},m_F),(g,\frac{7}{2},m_F)}, \tag{11}$$

$$\rho_{\mathrm{res}}^{\mathrm{2L}} = 1 - \sum_{m_F=-7/2}^{7/2}\rho_{(g,\frac{7}{2},m_F),(g,\frac{7}{2},m_F)}. \tag{12}$$

In the case of the one-laser scheme, the populations in the excited-state $F_e = 9/2$ manifold is taken out of the residual population, since atoms in that manifold can only decay in the ground-state $F_g = 7/2$ manifold: they will therefore be available for the retrapping sequence. Following a similar argument, when we calculate P_I for the one-laser scheme, we add the population of the excited-state $|9/2,\, 9/2\rangle$ sublevel to the population of the ground-state $|7/2,\, 7/2\rangle$ sublevel. Indeed, in this scheme, the target state is not dark: once atoms have reached the target state, they keep being excited to the excited-state $|9/2,\, 9/2\rangle$ sublevel, and they will have no choice but to decay back into the target state once the pumping laser is turned off. This of course implies that the optical pumping light should be turned off when the polarization is measured in the one-laser scheme, which is not necessary in the two-laser scheme.

3. Nuclear alignment

Since ^{35}Ar atoms have a nuclear spin greater than 1/2, they have additional degrees of freedom, which are associated

with the second moment of the nuclear spin [8]. As far as the angular distribution (4) is concerned, this means that a $\cos^2\theta$ term proportional to the nuclear alignment will appear [37]. For the sake of completeness, we therefore also keep track of the nuclear alignment of our sample.

We characterize the nuclear alignment by the quantity [53]

$$T_I = \frac{1}{I(2I-1)} \sum_{F=1/2}^{7/2} \sum_{m_F=-F}^{+F} \alpha_2(F, m_F)\rho_{(g,F,m_F),(g,F,m_F)}, \tag{13}$$

with

$$\alpha_2(F, m_F) = 3\langle I_z^2 \rangle_{|F,m_F\rangle} - I(I+1). \tag{14}$$

T_I is normalized in such a way that $T_I = +1$ (-1) corresponds to maximum prolate (oblate) alignment, i.e., all spins parallel (perpendicular) to the quantization z axis [53].

C. Atom-field interaction

To study the interaction of the atoms with the laser fields, we adopt the semiclassical approach, in which the atoms are treated quantum mechanically while the fields are treated classically. The time evolution of the atomic density operator $\hat{\rho}$ is given by the Liouville-von Neumann equation [25,54],

$$\dot{\hat{\rho}} = \frac{1}{i\hbar}[\hat{H}, \hat{\rho}] - \frac{1}{2}\{\hat{\Gamma}, \hat{\rho}\} + \mathrm{Tr}[\hat{\mathcal{F}}\hat{\rho}], \tag{15}$$

where $\hat{H}$ is the total Hamiltonian describing the composite system, i.e.,

$$\hat{H} = \hat{H}_A + \hat{H}_B + \hat{H}_L, \tag{16}$$

with $\hat{H}_A$ the atomic Hamiltonian, $\hat{H}_B$ the magnetic-field-atom-interaction Hamiltonian, and $\hat{H}_L$ the light-atom-interaction Hamiltonian, the curly brackets denote the anticommutator $\{\hat{A}, \hat{B}\} = \hat{A}\hat{B} + \hat{B}\hat{A}$, $\hat{\Gamma}$ is the relaxation operator, $\hat{\mathcal{F}}$ is the spontaneous emission operator, and the trace is taken over the excited-state pairs [54]. The last two terms in Eq. (15) are phenomenological terms added by hand to account for relaxation and repopulation mechanisms due to the interaction of the atomic system with its environment. In the following, the notation used to designate the elements of the atomic density matrix ρ will be adapted to the required level of specificity. A generic density matrix element will be referred to as ρ_{mn}, where m and n are shorthand notations for any two sublevels of the atomic system.

In our model, we only consider intrinsic relaxation of excited states due to spontaneous emission, but the relaxation operator $\hat{\Gamma}$ may be further developed to include terms due to collisions and transit relaxation [25,54]. The matrix associated with the relaxation operator is a Hermitian diagonal matrix whose diagonal elements are the spontaneous decay rates of the states (zero for ground-state sublevels and $\Gamma \equiv 1/\tau$, where τ is the lifetime of the transition, for excited-state sublevels). Let $\{g\}$ ($\{e\}$) denotes the subset of ground-state (excited-state) sublevels. Calculating the anticommutator in Eq. (15) for a given density matrix element ρ_{mn}, one obtains

$$\{\hat{\Gamma}, \hat{\rho}\}_{mn} = \begin{cases} 2\Gamma\rho_{mn}, & \text{if } m, n \in \{e\} \\ 0, & \text{if } m, n \in \{g\} \\ \Gamma\rho_{mn}, & \text{if } m \in \{e\}, n \in \{g\} \\ & \text{or vice versa.} \end{cases} \tag{17}$$

Intrinsic relaxation of excited-state sublevels and repopulation of ground-state sublevels go hand in hand. The latter process is described by the spontaneous-emission operator $\hat{\mathcal{F}}$. The rate of change of a given ground-state density matrix element ρ_{mn} due to this process is given by [25]

$$\begin{aligned} \dot{\rho}_{mn}^{(\mathrm{repop})} &= \sum_{r,s} \frac{\omega_0^3}{3\pi\epsilon_0\hbar c^3} \mathbf{d}_{mr} \cdot \mathbf{d}_{sn}\, \rho_{rs} \\ &\equiv \sum_{r,s} \mathcal{F}_{mn}^{sr}\, \rho_{rs} = \mathrm{Tr}(\hat{\mathcal{F}}_{mn}\hat{\rho}_e), \end{aligned} \tag{18}$$

where $\mathcal{F}_{mn}^{rs}$ connects a pair of excited states r and s to a pair of ground states m and n, $\hat{\rho}_e$ is the excited-state density operator, and the trace is taken over the pairs of excited states. The matrix representing the spontaneous-emission operator $\hat{\mathcal{F}}$ is a matrix of matrices [25]: each element of the outer matrix is itself a matrix. The outer matrix is expressed in the basis of the ground states referred to by the lower indices of $\mathcal{F}_{mn}^{rs}$, while each inner matrix is expressed in the basis of the upper states corresponding to the upper indices.

Applying Eq. (15) to the density operator describing our system (see Fig. 1) yields a set of 2034 coupled differential equations, the so-called optical Bloch equations. Since ρ is Hermitian and of unit trace, the number of independent equations is reduced to 1175. The optical Bloch equations are solved within the rotating-wave approximation.

With circularly polarized light, the density matrix elements decouple into subgroups, which can lead to significant simplification of the optical Bloch equations. In our calculations, the off-diagonal elements (i.e., the coherences) are initially taken to be equal to zero. Only some of the diagonal elements (i.e., the populations) have an initial nonzero value – we start with an initial equidistribution of the populations in the $F_g = 7/2$ manifold. In other words, if off-diagonal elements are decoupled from the diagonal elements, they can simply be left out of the calculations. For σ^+ light, the density matrix elements decouple into 15 subgroups, as illustrated in Fig. 3. One of them contains the populations as well as two types of coherences: the optical coherences for which $\Delta m_F = +1$ and the hyperfine coherences for which $\Delta m_F = 0$. We are therefore left with 290 equations, and we keep them all, thus taking into account the eight hyperfine levels of the $4s[3/2]_2 \rightarrow 4p[5/2]_3$ transition (see Fig. 1) and making our model sensitive to population losses to levels not addressed by the laser beams.

IV. RESULTS

We investigate the effect of both the magnetic field amplitude B and the saturation parameter s (i.e., the laser intensity) on the internal dynamics of the atomic ensemble. We explore a range of values for B such that the Zeeman splittings remain much smaller than the other energy intervals. For the sake of readability and for ease of comparison, the degree of

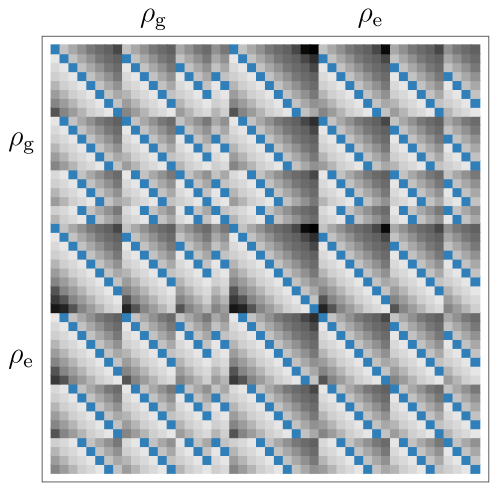

FIG. 3. Grouping of the density matrix elements when the atomic system interacts with σ^+ light. The elements in blue belong to the group, which is kept in our simulations. These elements are all coupled to the populations, i.e., the only matrix elements that are initially nonzero. The various shades of gray correspond to the 14 other groups of coupled elements.

polarization P_I is presented as $1 - P_I$ in the figures illustrating our results.

Obviously, knowing that a given degree of polarization can be achieved has not real interest if we do not monitor both the interaction time needed to reach it and the resulting population distribution among the different hyperfine manifolds. In the following, we give the degree of polarization as well as the residual population after an interaction time of 140 μs. First, we numerically observed that, within such an interaction time, both the one-laser and the two-laser schemes could achieve high degrees of polarization for a variety of (B, s) parameters, thus allowing for a comparison of the various schemes against a common backdrop. Second, the order of magnitude of this timescale agrees with that used in existing experimental setups, e.g., in Ref. [8], where ^{37}K atoms were measured to have reached maximal polarization after an interaction time of 100 μs. The fact that we are considering trapped atoms is crucial there: while longer interaction times would enable us to achieve higher degrees of polarization, they would also make recapturing the atoms harder. In order to complement this, we also provide the time evolution of the degree of polarization for two sets of (B, s) parameters, which enables one to appreciate how the time efficiency of the various schemes compare in different regimes.

As mentioned in Sec. II, the nuclear spin polarization should at least be measured to a precision of 0.5% so as to make sure that the uncertainty on the nuclear spin polarization does not dominate the uncertainty on A_β. We also noted that reaching $1 - P_I = 10^{-2}$ and measuring it to a relative precision of 20% would yield a relative uncertainty $\Delta P_I/P_I = 0.2\%$. Does this mean that we should be satisfied if the studied schemes manage to reach $1 - P_I = 10^{-2}$? Not quite. Our model focuses on an ideal, well-controlled situation: even though it includes population losses due to nonresonant excitations, it does not account for other mechanisms that can limit the efficiency of optical pumping, such as imperfections in the circular polarization of the pumping light and the presence of a transverse magnetic field [8,9]. This prompts us to adopt a conservative approach and set a goal threshold at 10^{-4}.

A. One-laser scheme

In the one-laser simulations, the laser frequency is tuned to $\nu_{g,7/2}^{e,9/2}$ no matter the value of the magnetic field B. In other words, it is not fine tuned so as to take into account Zeeman shifts. In such a way, no transition starting from the sublevels in the $F_g = 7/2$ manifold is favored, which is particularly interesting at the beginning of the optical pumping sequence.

We show in Fig. 4 that, after an interaction time of 140 μs, the fractional population remaining out of the target state space is kept below 10^{-4}; the precise value depends on the chosen regime of parameters (B, s). Full polarization within 10^{-4} of the sample can therefore be achieved while keeping population losses below 10^{-4}. The amplitude of the static magnetic field is not critical to achieving efficient optical pumping. Instead, larger values of B lead to larger detunings, which results in poorer efficiency in terms of pumping speed. As can be expected, optical pumping is faster when the laser intensity is increased. However, it is to be noted that we willingly restricted our calculations to low intensities in order to limit heating effects as much as possible. In addition, when the saturation parameter is kept low, the fraction of atoms lost to inferior ground-state hyperfine manifolds is slightly smaller.

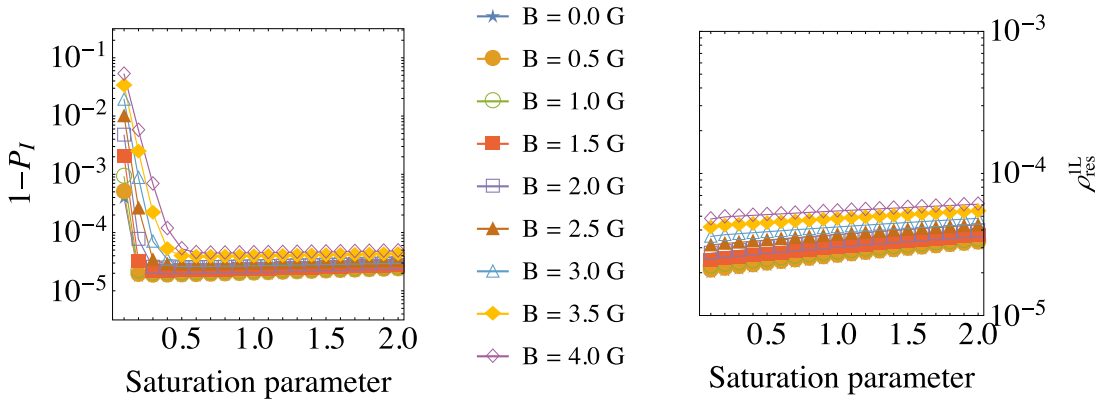

FIG. 4. (One-laser scheme.) Final nuclear polarization degree P_I and final residual population $\rho_{\text{res}}^{1\text{L}}$ after an interaction time of 140 μs.

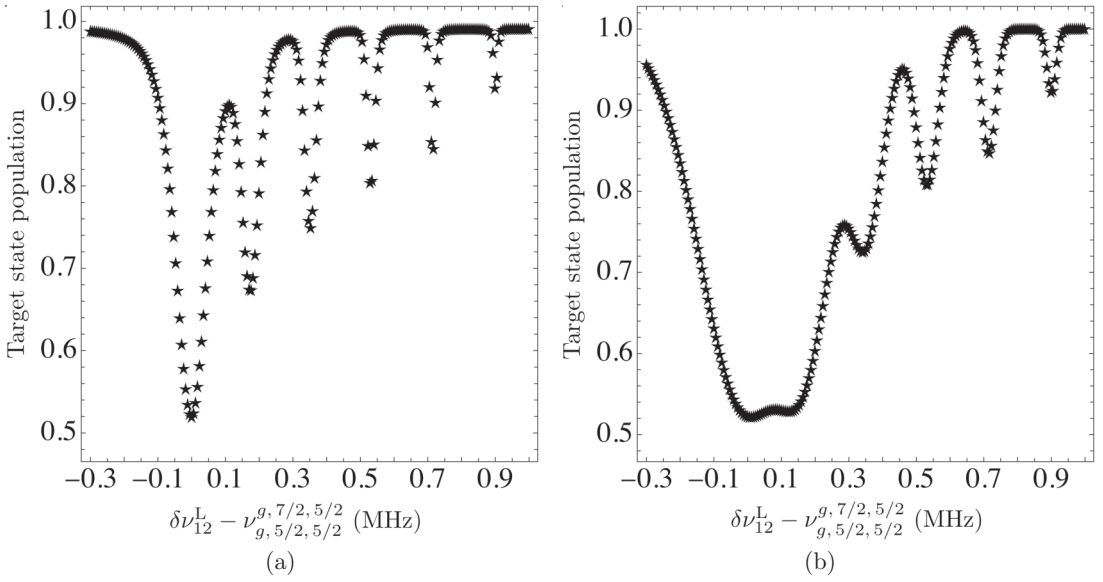

FIG. 5. (Two-laser scheme.) CPT spectrum for $B = 1.5$ G, $t_{\mathrm{int}} = 140$ μs, and (a) $s \equiv s_1 = s_2 = 0.1$, (b) $s = 1$.

The same observation also holds for the amplitude of the static magnetic field.

B. Two-laser scheme

As mentioned earlier, one needs to be careful with the laser frequencies in the two-laser scheme. On the one hand, the frequency difference between the two lasers has to be safely detuned from any CPT resonances. On the other hand, the relatively weak line strength of the $F_g = 7/2 \rightarrow F_e = 7/2$ transition needs to be compensated by a well-considered choice of the detuning of the pumper: the closer to the addressed transition, the better.

Ultimately, the target transition that the pumper needs to address is the $|7/2, {}^{+5}/2\rangle \rightarrow |7/2, {}^{+7}/2\rangle$ transition, while the ultimate target transition of the repumper is the $|5/2, {}^{+5}/2\rangle \rightarrow |7/2, {}^{+7}/2\rangle$ transition. The question therefore arises whether it is advantageous to favor these transitions from the very beginning of the optical pumping sequence. Obviously, both lasers should not be tuned to their ultimate respective target transitions, since the frequency difference $\delta\nu_{12}^{\mathrm{L}}$ would then be equal to the splitting between the ground-state Zeeman sublevels $|5/2, {}^{5}/2\rangle$ and $|7/2, {}^{5}/2\rangle$, hence it would match a CPT resonance condition, namely $\delta\nu_{12}^{\mathrm{L}} = \nu_{g,5/2,5/2}^{g,7/2,5/2}$.

For example, when $B = 1.5\,\mathrm{G}$, $\nu_{g,5/2,m_F}^{g,7/2,m_F}$ ranges from 1006.15 MHz to 1007.05 MHz for $m_F = -5/2$ to $5/2$. The corresponding CPT resonance landscape is represented in Fig. 5(a) for two values of the saturation parameter s. Starting from the left, the resonances correspond, respectively, to

$$\delta\nu_{12}^{\mathrm{L}} = \nu_{g,5/2,m_F}^{g,7/2,m_F}, \text{ with } m_F \text{ ranging from } \tfrac{5}{2} \text{ to } -\tfrac{5}{2}.$$

Therefore, if one of the two laser beams is not detuned from resonance, we may expect–and we indeed observe optical pumping to be suboptimal in this regime. To counterbalance this effect and destroy the CPT condition, we introduce an extra detuning $\delta\nu$. In the results presented here, this extra detuning is applied to the repumper. We also considered a variation in which the extra detuning $\delta\nu$ is spread on both lasers: both are then detuned from the target transition by $\delta\nu/2$. However, in that case, the advantage of shifting the value of $\delta\nu_{12}^{\mathrm{L}}$ is outweighed by the drawback of reducing the efficiency of optical pumping on the $F_g = 7/2 \rightarrow F_e = 7/2$ transition. Since this situation does not lead to any improvement of the efficiency, we do not explicitly include the associated results in the following. As for the value of $\delta\nu$, we tested a range of them and noticed that an extra detuning of $+1$ MHz was sufficient to destroy the CPT condition, which agrees with Ref. [9]. As a consequence, when $\delta\nu$ is used, $\delta\nu_{12}^{\mathrm{L}}$ is slightly blue shifted with respect to the hyperfine ground-state splittings between the $F_g = 5/2$ and the $F_g = 7/2$ manifolds.

Table I summarizes the three variations of the two-laser scheme that we investigated and whose efficiencies we compared. In scheme 2A, the laser frequencies are both tuned in the same way as in the one-laser simulations. The pumper is tuned to the hyperfine $F_g = 7/2 \rightarrow F_e = 7/2$ transition, while the repumper is tuned to the hyperfine $F_g = 5/2 \rightarrow F_e = 7/2$ transition. As a result, the frequency difference $\delta\nu_{12}^{\mathrm{L}}$ falls in the range of the CPT resonances. In scheme 2B, the frequency of the pumper is left unchanged, but the frequency of the repumper is detuned by an amount $\delta\nu$ from the hyperfine transition that it addresses. As a result, $\delta\nu_{12}^{\mathrm{L}}$ is shifted, thus destroying the CPT condition. In scheme 2C, the two lasers are finely tuned to the ultimate target transitions that they are meant to address, i.e., the $|7/2, {}^{+5}/2\rangle \rightarrow |7/2, {}^{+7}/2\rangle$ transition for the pumper and the $|5/2, {}^{+5}/2\rangle \rightarrow |7/2, {}^{+7}/2\rangle$ for the

TABLE I. Three two-laser scheme configurations investigated here (see text).

	ν_1^{L}	ν_2^{L}	$\Rightarrow \delta\nu_{12}^{\mathrm{L}}$
2A	$\nu_{g,7/2}^{e,7/2}$	$\nu_{g,5/2}^{e,7/2}$	$\nu_{g,5/2}^{g,7/2}$
2B	$\nu_{g,7/2}^{e,7/2}$	$\nu_{g,5/2}^{e,7/2} + 1$ MHz	$\nu_{g,5/2}^{g,7/2} + 1$ MHz
2C	$\nu_{g,7/2,5/2}^{e,7/2,7/2}$	$\nu_{g,5/2,5/2}^{e,7/2,7/2} + 1$ MHz	$\nu_{g,5/2,5/2}^{g,7/2,5/2} + 1$ MHz

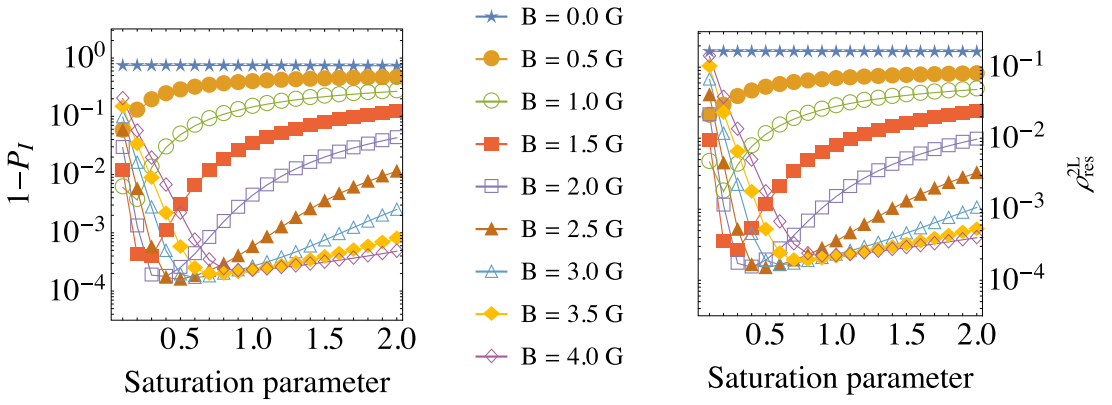

(a) Scheme 2A

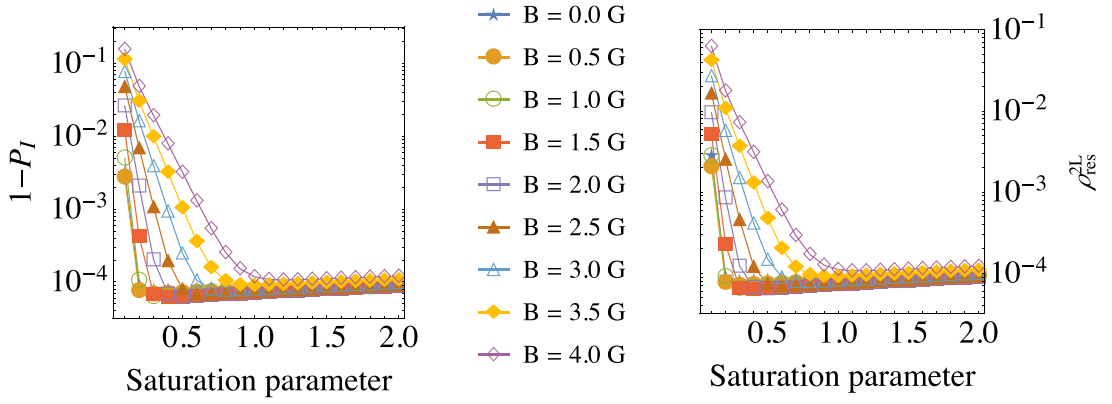

(b) Scheme 2B

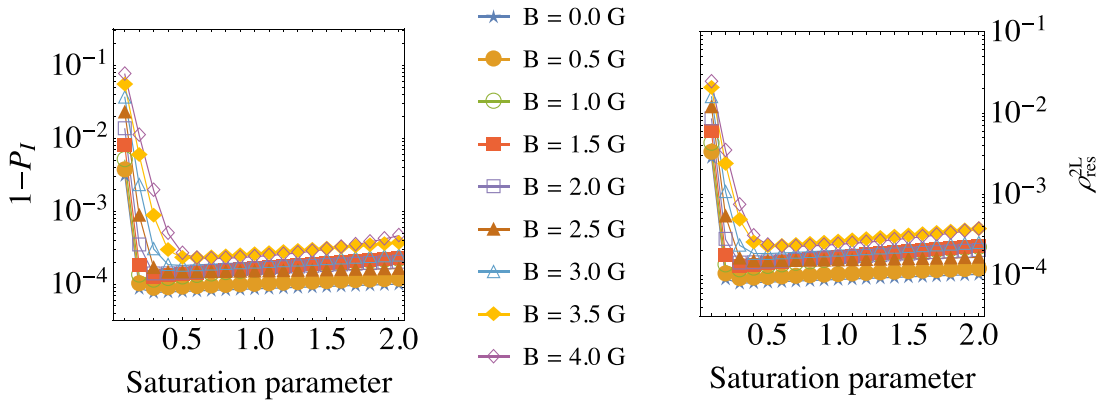

(c) Scheme 2C

FIG. 6. (Two-laser scheme situations B and C.) Final nuclear polarization degree P_I and final residual population $\rho_{\rm res}^{\rm 2L}$ after an interaction time of 140 μs. For schemes 2B and 2C: $\delta\nu = 1$ MHz (see text).

repumper. To avoid CPT effects, the repumper is then detuned from its ultimate target transition. We also considered a fourth situation in which the detuning is spread on both lasers: both are detuned from their target transition by $\delta\nu/2$.

As illustrated by Fig. 6, scheme 2B is more efficient when it comes to minimize the residual fractional population out of the target state space: it makes it possible to almost reach the levels reached when using the one-laser scheme. In contrast, scheme 2A leads to significant population loss. The efficiency of schemes 2A and 2C is far more dependent on the values of B and s than what is obtained with both scheme 2B and the one-laser scheme. This is true both in terms of final polarization and in terms of final residual population. Whereas the residual population $\rho_{\rm res}^{\rm 2L}$ can be kept around 10^{-4} with scheme 2B, its value when using schemes 2A and 2C is highly dependent on B and s, as is clear in Fig. 6. As far as polarization is concerned, the regions of the parameter space (B, s) where it is possible to achieve a high degree of polarization, i.e., where it is possible to reach the goal threshold of 10^{-4}, are slightly broader when using scheme 2B. Even though a well-chosen regime of (B, s) can lead to encouraging results using scheme 2A, the overall efficiency of this scheme is poorer than that of the two other two-laser schemes and is expected to be less robust once depolarizing mechanisms are

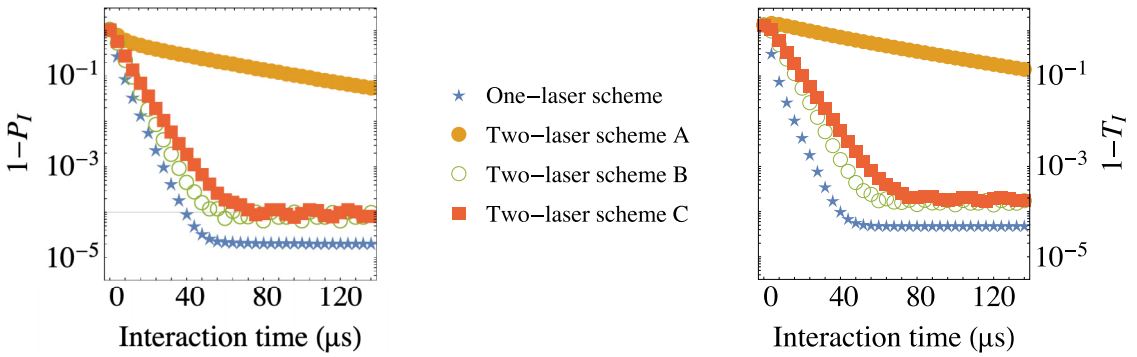

(a) $B = 1\,\mathrm{G}, s = 0.5$

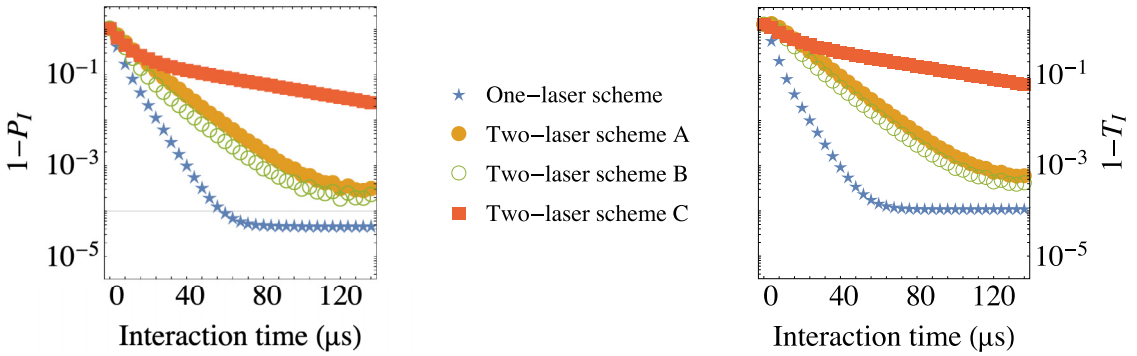

(b) $B = 4\,\mathrm{G}, s = 1$

FIG. 7. Time evolution of the nuclear polarization degree P_I and of the normalized nuclear alignment T_I.

taken into account. Such a variation in efficiency arises from the value of the frequency difference between the two lasers. In scheme 2B, the repumper is detuned from resonance, but the tradeoff is that the system is shielded from CPT effects, which are detrimental to optical pumping. Moreover, when the detuning of the repumper is positive, it mitigates the effects of the Zeeman shifts. As for whether it is advantageous to favor the target transitions from the very beginning of the optical pumping sequence, the comparison of schemes 2B and 2C indicates that the potential gains are counterbalanced by an increase in population losses and a narrower set of efficient (B, s) parameters.

As for the relative speed of the four schemes, it is illustrated in Fig. 7, which displays the time evolution of both P_I and T_I. It is noteworthy that time efficiency is tightly dependent on the values of the (B, s) parameters. Even though the overall speed of the one-laser scheme is better than than of the two-laser schemes, Fig. 7(a) makes it clear that a well-considered choice for (B, s) can bring the time efficiency of schemes 2B and 2C close to that of the one-laser scheme. Conversely, Fig. 7(b) provides an example where the gap in time efficiency between the one-laser and two-laser schemes is far bigger.

V. CONCLUSIONS

Comparing the efficiency of the various two-laser schemes makes it clear that CPT effects should be avoided at all costs. Whether a CPT-free two-laser scheme is preferable to the one-laser scheme depends on the priorities of a given experiment. It is easier to minimize the required interaction time with the one-laser scheme, but we have shown that choosing wisely the values of (B, s) could significantly increase the time efficiency of the two-laser scheme. Our results therefore highlight that the two-laser scheme is an alternative method, which provides both a dark state and very good optical pumping efficiency.

The present work focused on the internal dynamics of the atomic ensemble, that is, we did not investigate how the optical pumping process affects the velocity and position of the atoms. As optical pumping is applied to a cloud of trapped atoms, the external dynamics of the system remains a relevant issue and would be worth investigating in an extension of this study. Substantial variations in the atomic velocity would make the detuning time-dependent, thus complicating the process. Note that the use of counterpropagating beams, as in Ref. [8], may prove useful in circumventing such problems and controlling heating effects. An interesting line of further research would therefore consist in including the external dynamics of the system so as to quantify the advantages of using a dark state and/or counterpropagating beams in terms of heating effects.

This work also motivates further developments of the model, namely the inclusion of depolarizing mechanisms. Moreover, even though scheme 2C does not perform better than scheme 2B, it is still worth looking into how the addressed transitions can be optimized. As more and more atoms are pumped towards the stretched state, it would make sense to specifically address transitions starting from sublevels whose

populations are increasing. One way to produce such an effect is to use a time-dependent magnetic field [52].

Another extension of this study would be to investigate how to precisely measure the polarization in a given setup. Such a measurement must be non destructive so that the β-asymmetry parameter can be observed in the very same atomic sample [8]. One way would be to monitor fluorescence as a function of time, even though this method may not be the most convenient when working with a relatively low number of atoms [8]. An alternative method, which is used by Fenker *et al.* [8,9] in their work on ^{37}K, is to probe the partially polarized or unpolarized atoms with photoionization. The measuring approach goes hand in hand with the reconstruction of the population distribution within the ground state, which stresses the importance of quantum-state preparation and determination [55,56].

ACKNOWLEDGMENTS

We thank the Interuniversity Attraction Poles Programme initiated by the Belgian Science Policy Office (BriX network P7/12) and the Belgian FNRS through IISN convention 4.4512.08 for financial support.

[1] N. Severijns and O. Naviliat-Cuncic, Phys. Scr. **T152**, 014018 (2013).
[2] M. Tanabashi *et al.* (Particle Data Group), Phys. Rev. D **98**, 030001 (2018).
[3] J. A. Behr and G. Gwinner, J. Phys. G: Nucl. Part. Phys. **36**, 033101 (2009).
[4] J. A. Behr and A. Gorelov, J. Phys. G: Nucl. Part. Phys. **41**, 114005 (2014).
[5] N. D. Scielzo, S. J. Freedman, B. K. Fujikawa, and P. A. Vetter, Phys. Rev. Lett. **93**, 102501 (2004).
[6] D. Melconian *et al.*, Phys. Lett. B **649**, 370 (2007).
[7] F. Fang, D. J. Vieira, and X. Zhao, Phys. Rev. A **83**, 013416 (2011).
[8] B. Fenker *et al.*, New J. Phys. **18**, 073028 (2016).
[9] B. Fenker *et al.*, Phys. Rev. Lett. **120**, 062502 (2018).
[10] H. Kawamura *et al.*, Hyperfine Interact. **236**, 53 (2015).
[11] B. Ohayon *et al.*, Hyperfine Interact. **239**, 57 (2018).
[12] M. González-Alonso, O. Naviliat-Cuncic, and N. Severijns, Prog. Part. Nucl. Phys. **104**, 165 (2019).
[13] N. Severijns and O. Naviliat-Cuncic, Annu. Rev. Nucl. Part. Sci. **61**, 23 (2011).
[14] O. Naviliat-Cuncic and M. González-Alonso, Ann. Phys. (Berlin) **525**, 600 (2013).
[15] A. A. Valverde, *Precision Measurements to Test the Standard Model and for Explosive Nuclear Astrophysics* (Springer, Berlin, 2019).
[16] J. C. Hardy and I. S. Towner, Ann. Phys. (Berlin) **525**, 443 (2013).
[17] J. C. Hardy *et al.*, EPJ Web Conf. **93**, 01001 (2015).
[18] I. S. Towner and J. C. Hardy, J. Phys. G. Nucl. Part. Phys. **29**, 197 (2003).
[19] J. C. Hardy and I. S. Towner, Phys. Rev. C **91**, 025501 (2015).
[20] J. C. Hardy and I. S. Towner, PoS **(CKM 2016)**, 028 (2016).
[21] H. Abele, Prog. Part. Nucl. Phys. **60**, 1 (2008).
[22] D. Počanić *et al.*, Phys. Rev. Lett. **93**, 181803 (2004).
[23] O. Naviliat-Cuncic and N. Severijns, Phys. Rev. Lett. **102**, 142302 (2009).
[24] J. D. Jackson, S. B. Treiman, and H. W. Wyld Jr., Phys. Rev. **106**, 517 (1957).
[25] M. Auzinsh, D. Budker, and S. M. Rochester, *Optically Polarized Atoms: Understanding Light-Atom Interactions* (Oxford University Press, Oxford, 2010).
[26] W. Happer, J. Yuan-Yu, and T. Walker, *Optically Pumped Atoms* (Wiley-VCH, New York, 2010).
[27] C. Cohen-Tannoudji and D. Guéry-Odelin, *Advances in Atomic Physics: An Overview* (World Scientific, Singapore, 2011).
[28] W. Gins *et al.*, Nucl. Instrum. Meth. Phys. Res. A **925**, 24 (2019).
[29] T. Ohtsubo, S. Roccia, N. J. Stone, J. R. Stone, C. Gaulard, U. Köster, J. Nikolov, G. S. Simpson, and M. Veskovic, J. Phys. G: Nucl. Part. Phys. **44**, 044010 (2017).
[30] D. Kameda *et al.*, AIP Conf. Proc. **980**, 283 (2008).
[31] H. Törnqvist *et al.*, Nucl. Instrum. Meth. Phys. Res. B **317**, 685 (2013).
[32] N. Severijns and B. Blank, J. Phys. G: Nucl. Part. Phys. **44**, 074002 (2017).
[33] N. Severijns, M. Tandecki, T. Phalet, and I. S. Towner, Phys. Rev. C **78**, 055501 (2008).
[34] E. Tiesinga *et al.*, The 2018 CODATA Recommended Values of the Fundamental Physical Constants, Web Version 8.1, 2020.
[35] I. S. Towner and J. C. Hardy, Rep. Prog. Phys. **73**, 046301 (2010).
[36] L. Hayen and N. Severijns, arXiv:1906.09870.
[37] S. B. Treiman, Phys. Rev. **110**, 448 (1958).
[38] J. Chen, J. Cameron, and B. Singh, Nuclear Data Sheets **112**, 2715 (2011).
[39] W. Vassen, C. Cohen-Tannoudji, M. Leduc, D. Boiron, C. I. Westbrook, A. Truscott, K. Baldwin, G. Birkl, P. Cancio, and M. Trippenbach, Rev. Mod. Phys. **84**, 175 (2012).
[40] N. Small-Warren and L. Chow Chiu, Phys. Rev. A **11**, 1777 (1975).
[41] H. Katori and F. Shimizu, Phys. Rev. Lett. **70**, 3545 (1993).
[42] G. Norlén, Phys. Scr. **8**, 249 (1973).
[43] H. Katori and F. Shimizu, Jpn. J. Appl. Phys. **29**, L2124 (1990).
[44] P. D. Edmunds and P. F. Barker, Phys. Rev. Lett. **113**, 183001 (2014).
[45] F. Ritterbusch, S. Ebser, J. Welte, T. Reichel, A. Kersting, R. Purtschert, W. Aeschbach-Hertig, and M. K. Oberthaler, Geophys. Res. Lett. **41**, 6758 (2014).
[46] W. Gins, Development of a dedicated laser-polarization beamline for ISOLDE-CERN, Ph.D. thesis, KU Leuven (Belgium) (2019).
[47] W. R. Johnson, Can. J. Phys. **89**, 429 (2011).
[48] J. Li, P. Jönsson, M. Godefroid, C. Dong, and G. Gaigalas, Phys. Rev. A **86**, 052523 (2012).
[49] M. Walhout, A. Witte, and S. L. Rolston, Phys. Rev. Lett. **72**, 2843 (1994).

[50] F. Atoneche and A. Kastberg, Eur. J. Phys. **38**, 045703 (2017).
[51] S. Gu, J. A. Behr, M. N. Groves, and D. Dhat, Opt. Commun. **220**, 365 (2003).
[52] S. J. Park, T. Shin, J. H. Lee, G. D. Kim, and Y. K. Kim, J. Opt. Soc. Am. B **31**, 2278 (2014).
[53] G. Neyens, Rep. Prog. Phys. **66**, 633 (2003).
[54] M. Auzinsh, D. Budker, and S. M. Rochester, Phys. Rev. A **80**, 053406 (2009).
[55] B. Wang, Y. Han, J. Xiao, X. Yang, C. Zhang, H. Wang, M. Xiao, and K. Peng, Phys. Rev. A **75**, 051801(R) (2007).
[56] P. London, O. Firstenberg, M. Shuker, and A. Ron, Phys. Rev. A **81**, 043835 (2010).